Silicon-rich nitride waveguides for ultra-broadband nonlinear signal processing

Research Article | Vol. 25, No. 11 | 29 May 2017 | OPTICS EXPRESS 12100
Optics EXPRESS

Silicon-rich nitride waveguides for ultra-broadband nonlinear signal processing

MOHAMMAD REZAGHOLIPOUR DIZAJI,[1,3] CLEMENS J. KRÜCKEL,[2] ATTILA FÜLÖP,[2] PETER A. ANDREKSON,[2] VICTOR TORRES-COMPANY,[2] AND LAWRENCE R. CHEN[1,*]

[1]*Department of Electrical and Computer Engineering, McGill University, Montreal, Quebec, H3A0E9, Canada*
[2]*Department of Microtechnology and Nanoscience (MC2), Chalmers University of Technology, 41296 Gothenburg, Sweden*
[3]*mohammad.rezagholipourdizaji@mail.mcgill.ca*
[*]*lawrence.chen@mcgill.ca*

Abstract: Silicon nitride (Si_xN_y) waveguides constitute a technology platform to realize optical signal processing based on the nonlinear Kerr effect. Varying the stoichiometry of the core (i.e., x and y in silicon nitride) provides an additional degree of freedom for engineering the waveguide properties, such as nonlinear Kerr parameter and dispersion. We demonstrate low-stress high-confinement silicon-rich nitride waveguides with flat and anomalous dispersion over the entire *C* and *L* optical wavelength transmission bands for optical signal processing based on cross-phase modulation. The waveguides do not show any nonlinear loss for a measured optical input intensity of up to 1.5×10^9 W/cm^2. In particular, we achieve wavelength conversion of 10 Gb/s signals across the C band; XPM broadening is also observed in the *O* band. In addition, we highlight the use of Si_xN_y waveguides for nonlinear microwave photonics. Specifically, we demonstrate radio-frequency spectral monitoring of optical signals with a bandwidth of hundreds of gigahertz.

OCIS codes: (130.3120) Integrated optics devices; (130.7405) Wavelength conversion devices; (060.4510) Optical communications; (060.5625) Radio frequency photonics.

References and links

1. L. Yan, A. E. Willner, X. Wu, A. Yi, A. Bogoni, Z.-Y. Chen, and H.-Y. Jiang, "All-optical signalprocessing for ultrahigh speed optical systems and networks," J. Lightwave Technol. **30**(24), 3760–3770 (2012).
2. A. E. Willner, S. Khaleghi, M. R. Chitgarha, and O. F. Yilmaz, "All-optical signal processing," J. Lightwave Technol. **32**(4), 660–680 (2014).
3. Z. Li, Y. Dong, J. Mo, Y. Wang, and C. Lu, "Cascaded all-optical wavelength conversion for RZ-DPSK signal based on four-wave mixing in semiconductor optical amplifier," IEEE Photonics Technol. Lett. **16**(7), 1685–1687 (2004).
4. T. Tanemura, C. S. Goh, K. Kikuchi, and S. Y. Set, "Highly efficient arbitrary wavelength conversion within entire C-band based on nondegenerate fiber four-wave mixing," IEEE Photonics Technol. Lett. **16**(2), 551–553 (2004).
5. R. Espinola, J. Dadap, R. Osgood, Jr., S. McNab, and Y. Vlasov, "C-band wavelength conversion in silicon photonic wire waveguides," Opt. Express **13**(11), 4341–4349 (2005).
6. M. A. Foster, A. C. Turner, R. Salem, M. Lipson, and A. L. Gaeta, "Broad-band continuous-wave parametric wavelength conversion in silicon nanowaveguides," Opt. Express **15**(20), 12949–12958 (2007).
7. J. P. R. Lacey, G. J. Pendock, and R. S. Tucker, "All-optical 1300-nm to 1550-nm wavelength conversion using cross-phase modulation in a semiconductor optical amplifier," IEEE Photonics Technol. Lett. **8**(7), 885–887 (1996).
8. B. E. Olsson, P. Ohlen, L. Rau, and D. J. Blumenthal, "A simple and robust 40-Gb/s wavelength converter using fiber cross-phase modulation and optical filtering," IEEE Photonics Technol. Lett. **12**(7), 846–848 (2000).
9. V. G. Ta'eed, M. R. E. Lamont, D. J. Moss, B. J. Eggleton, D. Y. Choi, S. Madden, and B. Luther-Davies, "All optical wavelength conversion via cross phase modulation in chalcogenide glass rib waveguides," Opt. Express **14**(23), 11242–11247 (2006).
10. M. Galili, L. Oxenløwe, H. Mulvad, A. Clausen, and P. Jeppesen, "Optical wavelength conversion by cross-phase modulation of data signals up to 640 Gb/s," IEEE J. Sel. Top. Quantum Electron. **14**(3), 573–579 (2008).

#287786 https://doi.org/10.1364/OE.25.012100
Journal © 2017 Received 1 Mar 2017; revised 28 Apr 2017; accepted 2 May 2017; published 15 May 2017

Optics EXPRESS

11. W. Astar, J. B. Driscoll, X. Liu, J. I. Dadap, W. M. J. Green, Y. A. Vlasov, G. M. Carter, and R. M. Osgood, Jr., "Tunable wavelength conversion by XPM in a silicon nanowire, and the potential for XPM-multicasting," J. Lightwave Technol. **28**(17), 2499–2511 (2010).
12. J. Yao, "Microwave photonics," J. Lightwave Technol. **27**(3), 314–335 (2009).
13. C. Dorrer and D. N. Maywar, "RF spectrum analysis of optical signals using nonlinear optics," J. Lightwave Technol. **22**(1), 266–274 (2004).
14. M. Pelusi, F. Luan, T. D. Vo, M. R. E. Lamont, S. J. Madden, D. A. Bulla, D. Y. Choi, B. Luther-Davies, and B. J. Eggleton, "Photonic-chip-based radio-frequency spectrum analyser with terahertz bandwidth," Nat. Photonics **3**(3), 139–143 (2009).
15. J. Leuthold, C. Koos, and W. Freude, "Nonlinear silicon photonics," Nat. Photonics **4**(8), 535–544 (2010).
16. D. J. Moss, R. Morandotti, A. L. Gaeta, and M. Lipson, "New CMOS-compatible platforms based on silicon nitride and Hydex for nonlinear optics," Nat. Photonics **7**(8), 597–607 (2013).
17. C.-L. Wu, Y.-H. Lin, C.-H. Cheng, S.-P. Su, B.-J. Huang, J.-H. Chang, C.-I. Wu, C.-K. Lee, and G.-R. Lin, "Enriching Si quantum dots in a Si-rich SiN_x matrix for strong $\chi^{(3)}$ optical nonlinearity," J. Mater. Chem. **4**, 1405–1413 (2016).
18. B. J. Eggleton, B. Luther-Davies, and K. Richardson, "Chalcogenide photonics," Nat. Photonics **5**(3), 141–148 (2011).
19. J. F. Bauters, M. J. R. Heck, D. D. John, J. S. Barton, C. M. Bruinink, A. Leinse, R. G. Heideman, D. J. Blumenthal, and J. E. Bowers, "Planar waveguides with less than 0.1 dB/m propagation loss fabricated with wafer bonding," Opt. Express **19**(24), 24090–24101 (2011).
20. J. S. Levy, A. Gondarenko, M. A. Foster, A. C. Turner-Foster, A. L. Gaeta, and M. Lipson, "CMOS-compatible multiple-wavelength oscillator for on-chip optical interconnects," Nat. Photonics **4**(1), 37–40 (2010).
21. H. Philipp, K. N. Andersen, W. Svendsen, and H. Ou, "Amorphous silicon rich silicon nitride optical waveguides for high density integrated optics," Electron. Lett. **40**(7), 419–421 (2004).
22. C. J. Krückel, A. Fülöp, T. Klintberg, J. Bengtsson, P. A. Andrekson, and V. Torres-Company, "Linear and nonlinear characterization of low-stress high-confinement silicon-rich nitride waveguides," Opt. Express **23**(20), 25827–25837 (2015).
23. T. Barwicz, M. Popović, P. Rakich, M. Watts, H. Haus, E. Ippen, and H. Smith, "Microring-resonator-based add-drop filters in SiN: fabrication and analysis," Opt. Express **12**(7), 1437–1442 (2004).
24. Y.-H. Lin, C.-L. Wu, Y. H. Pai, and G. R. Lin, "A 533-nm self-luminescent Si-rich SiNx/SiOx distributed Bragg reflector," Opt. Express **19**(7), 6563–6570 (2011).
25. C.-D. Lin, C.-H. Cheng, Y.-H. Lin, C.-L. Wu, Y.-H. Pai, and G.-R. Lin, "Comparing retention and recombination of electrically injected carriers in Si quantum dots embedded in Si-rich SiN_x films," Appl. Phys. Lett. **99**(24), 243501 (2011).
26. T. Wang, D. K. T. Ng, S. K. Ng, Y. T. Toh, A. K. L. Chee, G. F. R. Chen, Q. Wang, and D. T. H. Tan, "Supercontinuum generation in bandgap engineered, back-end CMOS compatible silicon rich nitride waveguides," Laser Photonics Rev. **9**(5), 498–506 (2015).
27. C. Lacava, S. Stankovic, A. Khokhar, T. Dominguez, F. Gardes, D. J. Richardson, G. T. Reed, and P. Petropoulos, "CMOS-compatible silicon-rich nitride waveguides for ultrafast nonlinear signal processing," in *Conf. Laser and Electro-Optics* (2016), paper Stu4Q.7.
28. G.-R. Lin, S.-P. Su, C.-L. Wu, Y.-H. Lin, B.-J. Huang, H.-Y. Wang, C.-T. Tsai, C.-I. Wu, and Y.-C. Chi, "Si-rich SiN_x based Kerr switch enables optical data conversion up to 12 Gbit/s," Sci. Rep. **5**(1), 9611 (2015).
29. C.-L. Wu, Y.-H. Lin, S.-P. Su, B.-J. Huang, C.-T. Tsai, H.-Y. Wang, Y.-C. Chi, C.-I. Wu, and G.-R. Lin, "Enhancing optical nonlinearity in a nonstoichiometric SiN waveguide for cross-wavelength all-optical data processing," ACS Photonics **2**(8), 1141–1154 (2015).
30. C. Lacava, S. Stankovic, A. Z. Khokhar, T. D. Bucio, F. Y. Gardes, G. T. Reed, D. J. Richardson, and P. Petropoulos, "Si-rich silicon nitride for nonlinear signal processing applications," Sci. Rep. **7**(1), 22 (2017).
31. X. Liu, M. H. Pu, B. B. Zhou, C. J. Krückel, A. Fülöp, V. T. Company, and M. Bache, "Ocatve-spanning supercontinuum generation in a silicon-rich nitride waveguide," Opt. Lett. **41**(12), 2719–2722 (2016).
32. M. A. Galle, E. Y. Zhu, S. S. Saini, W. S. Mohammed, and L. Qian, "Characterizing short dispersion-length fiber via dispersive virtual reference interferometry," Opt. Express **22**(12), 14275–14284 (2014).
33. A. R. Motamedi, A. H. Nejadmalayeri, A. Khilo, F. X. Kärtner, and E. P. Ippen, "Ultrafast nonlinear optical studies of silicon nanowaveguides," Opt. Express **20**(4), 4085–4101 (2012).
34. T. D. Vo, M. D. Pelusi, J. Schröder, F. Luan, S. J. Madden, D.-Y. Choi, D. A. P. Bulla, B. Luther-Davies, and B. J. Eggleton, "Simultaneous multi-impairment monitoring of 640 Gb/s signals using photonic chip based RF spectrum analyzer," Opt. Express **18**(4), 3938–3945 (2010).
35. B. Corcoran, T. D. Vo, M. D. Pelusi, C. Monat, D. X. Xu, A. Densmore, R. Ma, S. Janz, D. J. Moss, and B. J. Eggleton, "Silicon nanowire based radio-frequency spectrum analyzer," Opt. Express **18**(19), 20190–20200 (2010).
36. M. Ferrera, C. Reimer, A. Pasquazi, M. Peccianti, M. Clerici, L. Caspani, S. T. Chu, B. E. Little, R. Morandotti, and D. J. Moss, "CMOS compatible integrated all-optical radio frequency spectrum analyzer," Opt. Express **22**(18), 21488–21498 (2014).

Optics EXPRESS

1. Introduction

In order to overcome the electronic bandwidth limitations in high-speed optical communication systems and networks, information should ideally be processed in the optical domain with no need for conversion into and from the electrical domain [1]. Over the years, all-optical signal processing has attracted interest, and a number of functionalities, such as reconfigurable add/drop multiplexing of high-speed optical time-division multiplexed signals, data grooming (e.g., equalization, optical regeneration, and flexible generation of advanced signals), and optical control of information (e.g., correlation and logic functions) have been demonstrated [2].

Wavelength conversion is an important nonlinear process that is often used to realize a variety of optical signal processing functions. Wavelength conversion can be obtained using different nonlinear effects such as four wave mixing (FWM) [3–6] or cross phase modulation (XPM) [7–11], and in a number of platforms, including highly nonlinear fibers [5,8], semiconductor optical amplifiers [4,11], chalcogenide waveguides [9] and silicon waveguides [3,6,10]. FWM-based wavelength conversion is transparent to the modulation format of the input data signal and can support advanced modulation formats. However, the wavelength conversion range may be constrained by the phase matching condition. On the other hand, XPM-based wavelength conversion has the advantage of broadband operation, although at the expense of only applying to amplitude modulation formats, and assuming the walk-off between the pump and the probe is properly controlled by dispersion engineering.

Another area of research that has attracted significant attention by the optical signal processing community is microwave photonics (MWP) [12], a discipline that gathers the two worlds of radio-frequency (RF) engineering and optoelectronics. This area of research is of particular interest mainly for the following two reasons: (1) functionalities that are not possible to be implemented directly in the radio-frequency domain (or at least very complex to be achieved) can be realized using MWP, and (2) new opportunities for information and communication systems and networks can be created using MWP. One of the MWP applications that highlights the potential of nonlinear optical effects to overcome the bandwidth limitation of electronics is the monitoring of the RF spectrum of an optical signal [13,14].

In all-optical signal processing and MWP applications, it will always be preferable to reduce the overall size of the photonics module/subsystem. As such, a number of different platforms, including chalcogenide and silicon, have been investigated to develop photonic integrated devices/circuits to perform signal processing. Historically, silicon-on-insulator (SOI) was the first silicon-based platform to be explored for nonlinear optical signal processing [15]. Recently, silicon nitride (Si_3N_4) has gained interest for integrated nonlinear optics [16,17]. Si_3N_4 has a wide transparency window from UV to short-wavelength infrared and therefore can operate over an ultrabroad wavelength range. For example, Si_3N_4 is more suitable for lightwave transmission applications in the near infrared compared to SOI as the latter has high absorption at wavelengths below 1100 nm. While Si_3N_4 has a lower nonlinear refractive index compared to chalcogenide [18] and SOI [15], the possibility of reducing the propagation loss (as low as 0.1 dB/m in thin waveguides was demonstrated in [19]) and the capability of handling high power levels make it an attractive platform for nonlinear optics. Most importantly, in contrast with SOI, Si_3N_4 is not expected to have nonlinear loss and two-photon absorption (TPA) in the telecommunication range due to its larger bandgap energy [20].

Varying the stoichiometry of the silicon nitride film provides an additional degree of freedom for engineering the waveguide properties. In particular, by increasing the silicon content of the film with respect to its stoichiometric form (Si_3N_4), the resulting structure has much lower stress [21]. This allows for growing thicker films and attaining anomalous dispersion in the C-band using single-core strip waveguides with standard silica cladding without compromising the device yield [22]. Silicon rich nitride (SRN) waveguides have been

Optics EXPRESS

extensively explored for linear optics [21,23–25] and recently gained momentum for nonlinear signal processing applications [22,26–30]. Our group has recently developed straight SRN waveguides based on low-pressure chemical vapor deposition [22]. The waveguides can be engineered to display broad and anomalous dispersion, leading to octave-spanning supercontinua when pumped with sub-kW femtosecond pulses from an erbium-fiber laser oscillator [31]. The observation of massive broadening with relatively low peak power pulses suggests these waveguides are useful for optical signal processing with telecommunication class signals, which usually operate at high data rates.

In this paper, we report XPM-based wavelength conversion using a dispersion engineered SRN waveguide. Error free operation is obtained for wavelength conversion of RZ-OOK data signals at 10 Gb/s across the C-band. Additional experimental results show XPM occurring at 1310 nm which demonstrates the potential for ultra-broadband wavelength conversion. Measurements show no evidence of nonlinear loss in the telecommunication range. We also report the first operation of an XPM-based RF spectrum analyzer (RFSA) using an integrated silicon nitride waveguide. Measurements of electrical spectra for optical pulse trains with repetition rates from ~10 GHz to ~160 GHz are demonstrated. The measurement results show an estimated bandwidth of ~900 GHz for our photonic RFSA.

2. Optical characteristics of the low-stress SRN waveguide

The inset in Fig. 1(a) shows the cross-section of the SRN waveguide with dimensions 0.7 × 1.65 μm^2 and 2 cm in length. The waveguides are fabricated according to [22]. The waveguide core is surrounded with SiO_2 and the contrast in the refractive index results in high confinement of the optical field.

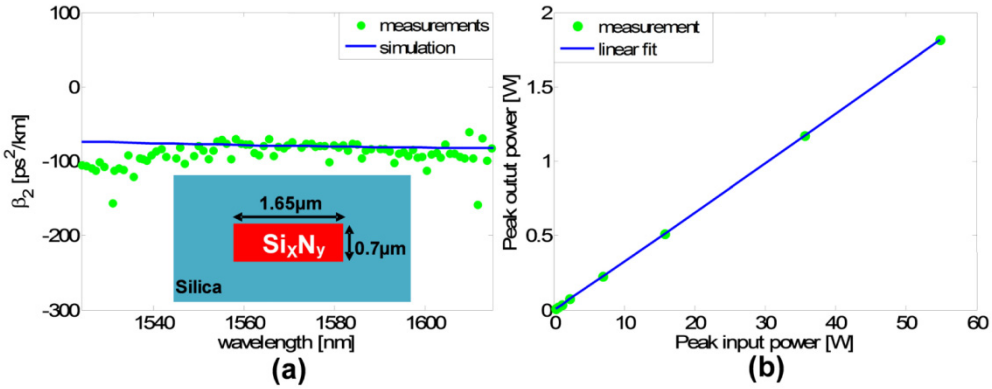

Fig. 1. Optical properties of the SRN waveguide: (a) Measured and simulated group velocity dispersion showing relatively flat and anomalousdispersion in the C&L bands. (b) Output received peak power vs. input launched peak power, showing negligible nonlinear loss. Inset: waveguide cross-section.

The waveguide supports both quasi-TE and quasi-TM modes and the overall fiber-to-fiber loss for the quasi-TE mode is ~14.7 dB using edge coupling into and out of the waveguide with lensed fibers of 2 μm spot size diameter. Owing to the rectangular symmetry of the waveguides, the fundamental TE and TM modes have a different modal distribution. The fundamental TM mode interacts more with the sidewalls and is likely to display more losses than the TE mode as the waveguide sidewalls exhibit greater roughness compared to the upper and lower surfaces [22]. We infer that we excite the TE mode in our experiments by maximizing the power throughput with a polarization controller, where we observe a polarization dependent loss of ~1 dB.

Figure 1(a) shows the measured and calculated group velocity dispersion coefficient (β_2) for the fundamental quasi-TE mode. The dispersion was measured using commercially

Optics EXPRESS

available dispersive virtual reference interferometer technology [32]. The measurement yields a relatively flat and anomalous parameter over the entire C- and L-bands with $\beta_2 = -77$ ps^2/km at 1550 nm.

In order to confirm the absence of nonlinear absorption for the SRN waveguide in the telecommunications band, we measured the output power as a function of input launched power; see Fig. 1(b). The experimental setup for this measurement is similar to that shown in Fig. 2 except for the absence of the probe signal branch. Also, the input signal was a train of non-modulated pulses with FWHM duration of 2 ps and a repetition rate of 10 GHz at 1550 nm. As can be seen, a linear relation between output received peak power (intensity) and input launched peak power (intensity) is maintained for peak input launched powers of up to ~55 W which is equivalent to the peak optical intensity of $\sim 1.5 \times 10^9$ W/cm^2 at the input of the waveguide (the maximum achieved from the laser). The peak input launched / output received power and the peak input / output intensity at the both ends of the waveguide are related to each other by taking into account an estimated 6 dB coupling loss at each facet of the waveguide, and also the 0.9 um^2 effective area of the waveguide. In the case of SOI, nonlinear absorption is observed at peak power of about few milliwatts [33]. This is expected since the bandgap energy of the SRN film is too large for TPA to occur at 1550 nm [22].

3. All-optical wavelength conversion experiments

3.1 Experimental setup

Figure 2 shows the experimental setup for XPM-based wavelength conversion. The principle is based on the nonlinear phase shift induced by a high power data signal (pump) onto a CW signal (probe), i.e. spectral sidebands containing information of the data signal are generated around the CW probe. A wavelength converted version of the data signal is obtained by extracting the newly generated spectrum about the CW probe (e.g., by rejecting the CW carrier using a notch filter) [8].

The 10 Gb/s RZ-OOK data signal was generated by modulating the output from the 10 GHz mode-locked laser using an electro-optic Mach Zehnder modulator (MZM) driven by a $2^{31} - 1$ pseudo-random bit sequence (PRBS). The modulated data signal was then amplified to 33 dB using a high power EDFA (EDFA1). The CW probe was generated using an external cavity tunable laser and then amplified using another amplifier (EDFA2). In order to reduce the out-of-band amplified spontaneous emission (ASE) noise, a 0.3 nm band-pass filter (BPF) was used. The resulting CW probe power was 16.7 dBm. We used separate polarization controllers for the data signal and CW probe to maximize their nonlinear interaction inside the waveguide. The two signals were combined using a wavelength division multiplexer (WDM) coupler (the data signal passed through the transmission port, which had a passband of 5 nm and wascentered at 1550 nm) before being launched into the SRN waveguide. The output of the waveguide was filtered using a programmable filter (PF, Finisar Wave Shaper WS-1000S). The PF acted as a notch filter with a rejection bandwidth of 0.3 nm centered at the CW probe and a total passband of 5 nm to extract the XPM-broadened spectrum. The wavelength converted signal then passed through a variable optical attenuator (VOA) before the receiver. The receiver comprised an amplifier providing a constant output power of 19.5 dBm, a tunable filter with a bandwidth of 5.3 nm to remove out-of-band ASE, and a photodiode.

Optics EXPRESS

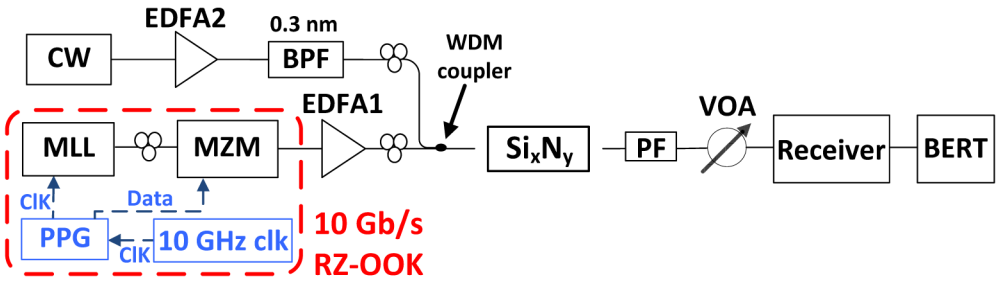

Fig. 2. Experimental setup for XPM-based wavelength conversion. PPG: pulse pattern generator. PF: programmable filter. BERT: bit error rate tester.

3.2 Results and discussion

Figure 3(a) shows the optical spectra at the output of the SRN waveguide for different CW probe wavelengths that span the *C* band. As can be seen, the spectrum is broadened significantly at all probe wavelengths. The BER is measured for 4 different wavelength converted signals at 1532 nm, 1535 nm, 1562 nm, and 1564 nm, see Fig. 3(b). The power penalty at 10^{-9} varies in the range between 1.6 dB and 3.4 dB for different CW wavelengths. The difference in the power penalty is mostly due to the difference in the gain profile of the EDFA at different CW wavelengths. The wavelength range in which BER measurements are reported is limited by the wavelength range of the EDFAs and various filters used in the experiment, not by the SRN waveguide. The insets in Fig. 3(b) show the electrical eye diagrams (captured using a 30 GHz electrical sampling module) at a BER = 10^{-9} for the wavelength converted signal at 1562 nm and the data signal in back-to-back (B2B).

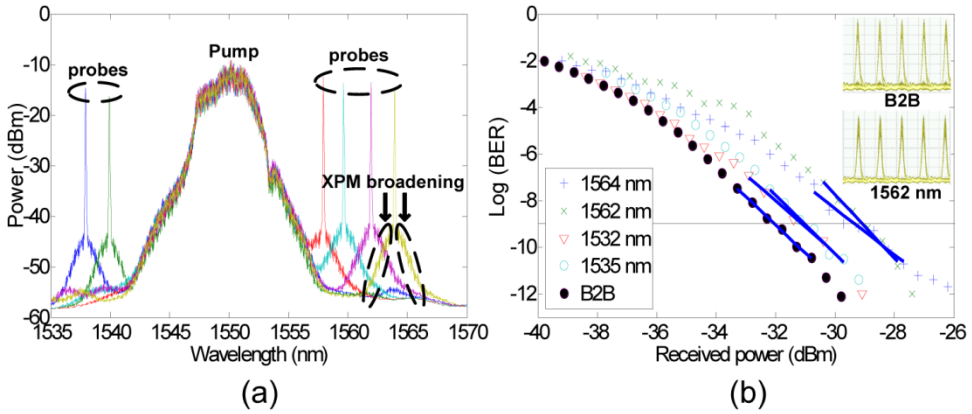

Fig. 3. (a) Optical spectra after the SRNwaveguide for different probe wavelengths. (b) BER for different wavelength-converted signals. Insets: electrical eye diagrams for the data signal (back-to-back) as well as the wavelength converted signal at 1562 nm for error-free operation (50 ps/div).

Next, we verified that XPM can take place over a significantly broader range by using a probe wavelength centered at 1310 nm. The experimental setup is similar to that in Fig. 2 except we use a 10 GHz pulse train rather than a modulated signal as the pump, since we could not perform BER measurement of data signals at the *O* band due to limitation of wavelength operation range of our equipment. The CW probe power was 14.5 dBm at 1310 nm. Figure 4 shows the optical spectra at the output of the SRN waveguide and XPM-broadening can be observed clearly, corresponding to a range spanning 240 nm.

Optics EXPRESS

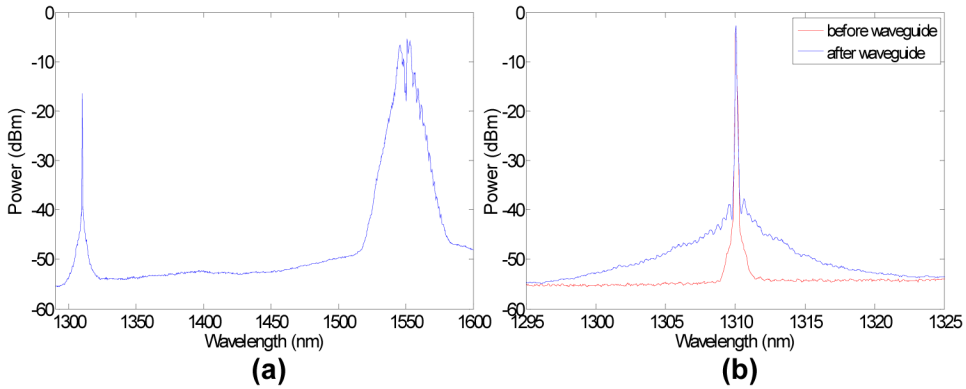

Fig. 4. (a) Optical spectrum at the output of the SRN waveguide showing XPM-based spectral broadening,(b) Zoom of the optical spectra at the input and output of the waveguide at the probe wavelength.

4. Photonic-assisted radio-frequency spectrum analyzer (RFSA)

The all-optical RFSA is based on the XPM interaction between the signal under test and a CW probe, such that the phase of the CW probe will be modulated by the intensity of the signal under test. This results in XPM-based spectral broadening about the CW probe's wavelength. This XPM-broadened spectral content of the optical spectrum centered at the CW probe can be recorded using an optical spectrum analyzer (OSA) and represents the RF spectrum of the signal under test [13]. The intrinsic bandwidth of the XPM-based RF spectrum analysis technique depends on the response time of the Kerr effect. In practice, the dispersion profile of the nonlinear medium will cause a walk-off between the probe and signal, ultimately limiting the bandwidth [13]. For low dispersive highly nonlinear devices, the photonic-based RFSA bandwidth is far beyond the speed of the state of the art electronics.The drawback of this technique is that the spectral resolution and dynamic range of the RFSA are limited by the OSA. Nevertheless, the bandwidth and spectral resolution allow for performance monitoring of T-baud telecommunication signals operating over long record lengths [34]. The photonic assisted RFSA has been demonstrated with HNLFs [13], and in diverse integrated platforms such as chalcogenide [14,34], silicon [35] and silica glass [36]. Implementing this technology with SRN could be useful for assessing waveforms in different regions of the electromagnetic spectrum.

4.1 Operation bandwidth characterization

The bandwidth of our RFSA is measured using the same procedure indicated in [13]. Briefly, it is based on the XPM interaction between a CW probe centered at the frequency f_p, and a set of two beating CW signals with a frequency separation Δf (around a center frequency f_s) that interact with the CW probe. The beating waves form a modulated envelope centered at the CW probe frequency with a detuning of Δf on both sides. By varying Δf and measuring the corresponding power amplitude of the tones at $f_p \pm \Delta f$ we can determine the operation bandwidthof our RFSA.

Figure 5(a) shows the experimental setup of the photonic RFSA. We use the same setup for measuring the estimated bandwidth of the photonic RFSA. For this purpose the block 'signal under test' comprises two tunable laser sources (TLS), with a frequency offset Δf with respect to each other which are then combined together using a 50/50 coupler. The combined signal (output of the 'signal under test' block) is amplified using a high power EDFA (EDFA 2) that can provide a maximum output power of 33 dBm. The CW probe signal is generated using a DFB laser source at 1538.9 nm which is amplified to 18 dBm followed by a BPF to remove the out of band ASE noise. The two signals are then combined and launched into the

Optics EXPRESS

SRN waveguide. The optical spectra of the output of the waveguide for different frequency detuning Δf were captured using an OSA.

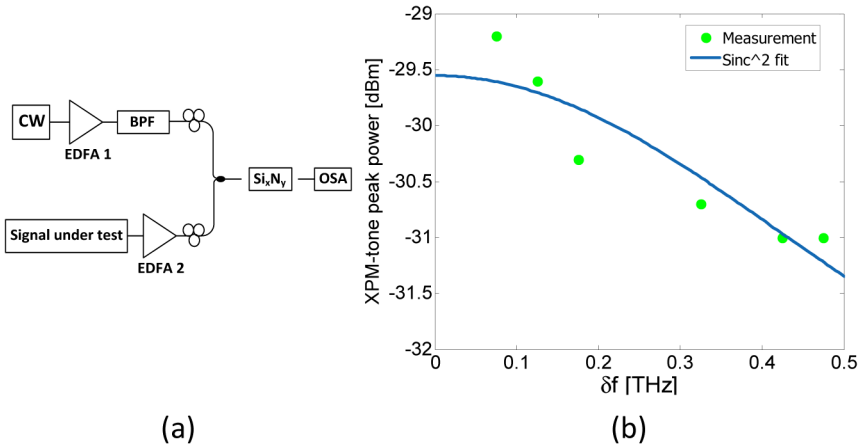

Fig. 5. (a) Experimental setup for the all-optical RF spectrum analyzer, CW: continuous wave, BPF: band pass filter, OSA: optical spectrum analyzer. (b) Bandwidth measurement results for the photonic RFSA showing the XPM-tone peak power as a function of frequency detuning Δf. The measurement data are fitted to a Sinc2 function for an estimation of the 3 dB bandwidth of the RF spectrum analyzer.

The bandwidth measurement results for the photonic RFSA are shown in Fig. 5(b). The measurement of the peak power of the XPM tones are performed for a frequency detuning of up to 470 GHz due to the limitation of our laser sources. The 1-dB bandwidth is ~350 GHz. However, form the sinc^2 fit [13] we estimate a 3-dB bandwidth of 0.9 THz, limited by the dispersion of the waveguide. The lower limit on the peak power of the source under test for which a measurable modulation on the spectrum can be obtained is ~6 dBm for our device. In the future designs of the SRN waveguide, we can also lower the dispersion by decreasing slightly the height of the core which would result in a larger bandwidth of operation of the RF spectrum analyzer [31].

4.2 RF spectra characterization of high-repetition-rate pulses

Next we demonstrate monitoring of the RF spectra of signals at rates of up to ~160 GHz using our photonic RFSA. The same experimental setup of the all-optical RFSA in Fig. 5(a) is used where in this case the signal under test is generated using the MLL from Sections 2 and 3 followed by passive multiplication of the repetition rate at 4 and 16 times using an optical multiplexer (OMUX). The output of the OMUX is passed through a polarization beam splitter in order to obtain a uniform polarization for all of the pulses at its output. The multiplexed signal is then amplified to ~27 dBm. Traces of the XPM spectrum obtained with a 20 MHz resolution OSA are shown in Fig. 6.

As can be seen the separation between the spectral lines is 9.95 GHz which is expected as it is equal to the repetition rate of the MLL. Figure 6(a) shows the measured RF spectrum for the original 9.95 GHz MLL generated pulse train, and Figs. 6(b) and 6(c) show the measured RF spectra for the pulse trains after repetition rate multiplication.

Optics EXPRESS

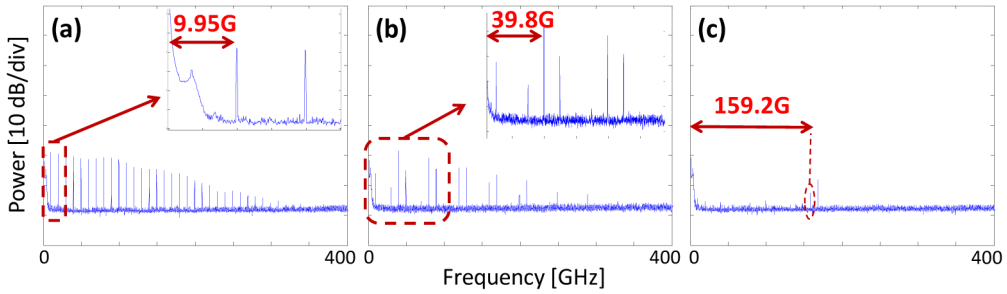

Fig. 6. Measured RF spectrum of pulse trains at (a) 9.95 GHz, (b) 39.8 GHz, (c) 159.2 GHz using a high resolution OSA with 20 MHz resolution.

Figures 6(b) and 6(c) show the existence of spurious tones at other frequencies in addition to the desired spectral tones of the corresponding pulse trains. This can be explained since the OMUX operates based on the passive multiplication of the repetition rate of the intensity of its input data signal using an interferometric structure. It is designed to receive a PRBS optical data signal with a pattern length of 2^7-1 at 9.95 GHz. It can multiply the data rate by either 4 or 16 at the output while preserving the pseudo randomness nature of the data signal, such that ideally the output data signal will remain a PRBS with the same pattern length of 2^7-1. However, instead of a data signal in our experiments, we used a pulse train at a repetition rate of 9.95 GHz as the input to the OMUX. Therefore, the output of the OMUX is not a pure multiplied version of the input pulse train and the corresponding spectrum of the output of the OMUX includes spurious tones at other frequencies, which is reflected on the recorded RF spectrum.

5. Conclusions

We have reported all-optical cross-phase modulation based processing of signal in the optical and microwave frequency regions using SRN waveguides. We demonstrate the feasibility for broadband nonlinear wavelength conversion from the O-band to the -C-band based on cross-phase modulation in a low-stress SRN waveguide. The waveguide, which is engineered to have flat and low dispersion over the C + L bands, does not display any nonlinear loss up to launched peak power levels of 55 W. BER measurements show error free operation for wavelength converted RZ-OOK signals at 10 Gb/s over the C-band. We also report the first demonstration of an XPM-based RFSA using an integrated silicon nitride waveguide. Measurements show an estimated bandwidth of hundreds of GHz for our RFSA. These results indicate that silicon nitride can be a powerful platform for performing photonic processing of microwave and optical signals.

Funding

Natural Sciences and Engineering Research Council (NSERC) of Canada Next-Generation Optical Networks CREATE program; the Swedish Research Council (VR); the Swedish Foundation for International Cooperation in Research and Higher Education (STINT).